# Hierarchical Anodic $TiO_2$ Nanostructures Formed in Ethylene Glycol/o-$H_3PO_4$ Electrolytes for Direct Photocatalysis

Laura Razzaboni,[a, c] Marco Altomare,[a] Mariapia Pedeferri,[c] Maria Vittoria Diamanti,[c] and Patrik Schmuki*[a, b]

In this work, we describe a simple anodization process of titanium in a hot phosphoric acid/ethylene glycol electrolyte that forms a hierarchically structured photocatalytically active $TiO_2$ layer that consists directly of anatase nanocrystallites. Such anodic layers show, without any annealing, a high photocatalytic degradation activity for AO7 (an azo-dye used as model pollutant) that is higher than the activity of comparable fully crystallized $TiO_2$ nanotube layers. Furthermore, the hierarchically structured layers have a remarkable mechanical bending stability. These features make these novel anodic layers highly promising for applications in flexible substrate based photocatalytic devices.

## 1. Introduction

Over the past decades, anodic self-organized $TiO_2$ nanotube (NT) layers[1–3] have become highly attractive for a large number of applications, such as photo-electrochemistry and photocatalysis,[4–6] solar-cells,[7–9] bioactive substrates or drug-delivery systems[10,11] among others.

Particularly the combination of $TiO_2$ intrinsic functionalities and a unique geometry that provides a high surface area and adjustable charge carrier management makes these nanotube layers interesting for any photon-harvesting device such as advanced photo-electrodes. A most straightforward application of $TiO_2$ NTs for photon-harvesting is in photocatalysis.[12] Photocatalytic processes are based on the absorption of light and the subsequent reaction of the generated charge carriers (conduction band electrons and valence band holes) with the environment (typically soluble red-ox species in an aqueous solution). In $TiO_2$, the exit energy of valence band holes is sufficiently high to oxidize virtually any organic compound finally to $CO_2$ and $H_2O$ – this effect has widely been used for the destruction of environmental pollutants, namely aromatic compounds, various pharmaceuticals, pesticides, or dyes.[13–15]

Generally, to obtain a high efficiency in photocatalytic degradation of pollutants (or model compounds such as AO7 dye), $TiO_2$ nanotubes need to be crystallized to the anatase phase. The as-grown anodic NT structures are amorphous and therefore they typically exhibit a poor performance. In order to achieve full crystallization, most commonly, amorphous nanotubes are thermally annealed in air at temperatures of 400–600 °C.[1] However, these annealing temperatures prohibit the application of $TiO_2$ NTs for flexible (plastic) electrodes. Therefore, methods such as so-called non-thickness-limited growth of partially crystalline mesoporous $TiO_2$ structures have attracted great interest.[16–18] Nevertheless, these procedures still are carried out at around 180–200 °C (in hot glycerol), while applications on flexible plastics require typically $T < 150$ °C. Therefore, anodization procedures that lead to crystalline or partially crystalline titania nanostructures at lower temperatures are highly desired.[19]

In the present work, we introduce an anodization process of Ti sheets that is carried out in an ethylene glycol/phosphate electrolyte at around 100 °C. We use as anodizing medium a mixture of pure molten ortho-phosphoric acid (o-$H_3PO_4$) containing small amount (5 vol%) of ethylene glycol (EG). Under optimized conditions, branched titania (hierarchical) nanostructures are formed that are partially crystallized to anatase and adhere extremely well to the metallic substrate. We test these structures in terms of their efficiency for the photocatalytic degradation of AO7 dye. We show that the here produced tree-like structures provide, as formed, a higher photocatalytic efficiency than fully crystallized titania nanotube layers.

[a] L. Razzaboni, Dr. M. Altomare, Prof. Dr. P. Schmuki
Department of Materials Science and Engineering, WW4-LKO
University of Erlangen-Nuremberg
Martensstrasse 7, 91058, Erlangen, Germany
E-mail: schmuki@ww.uni-erlangen.de
[b] Prof. Dr. P. Schmuki
Chemistry Department
King Abdulaziz University
80203 Jeddah, Kingdom of Saudi Arabia
[c] L. Razzaboni, Prof. Dr. M. Pedeferri, Prof. Dr. M. V. Diamanti
Department of Chemistry, Materials and Chemical Engineering "Giulio Natta"
Politecnico di Milano
Piazza Leonardo da Vinci 32, 20133 Milan, Italy

Supporting information for this article is available on the WWW under https://doi.org/10.1002/celc.202000673

## 2. Results and Discussion

Figure 1 a–d) show morphologies found after anodizing a titanium foil for various times in the ethylene glycol/phosphate electrolyte described in the experimental section, using a temperature of 105 °C and a voltage of 5 V. Clearly, an oxide layer is formed consisting of hierarchical "nanotrees" that increases in thickness with longer anodization times. The top view SEM images of such structures are shown in the supporting information in Figure S1. The lateral spacing of the individual tree-like structure is in the order of 50 nm or even lower, with branches of a thickness in the sub 5 nm range.

The current vs. time profile (for a structure grown after 24 h – Figure 1e) resembles in its shape the formation of other self-organized structures, such as anodic titania nanotubes[20,21] or pores in anodic alumina.[22] That is, in a first stage, initial self-organization takes place at current densities of several mA cm$^{-2}$, this then drops due to increasing oxide formation for a steady situation of current densities of a few mA cm$^{-2}$. This steady state is established due to a permanent oxide formation, likely a high field anodic process.

Similar current-time profiles for structures grown after 5 and 48 h are also shown in Figure S2. In every case, the various anodization stages can also be observed by clear changes in the electrolyte color, as shown in Figure S3. During the growth initiation, the electrolyte appears transparent while it turns pale yellow with increasing anodization time, this is probably due to formation of colored $Ti^{4+}$ complexes. Under steady state conditions the electrolyte gradually darkens, reaching a dark brown color in the late stages of anodization. This can be ascribed to a decomposition of the organic additive (ethylene glycol). In our case, this formation-dissolution equilibrium leads to layers of a thickness of approximately 1.4 μm after 24 h of anodization (Figure 1f).

XRD (Figure 2a) and HR-TEM (Figure 2b) of the anodic layer grown for 24 h confirm the formation of anatase during anodization, as evident from the diffraction peak at $2\theta = 25.1°$ that can be ascribed to the $TiO_2$ anatase (101) reflection. From the TEM, crystalline domains of approximately 5 nm in size can be identified with lattice fringes with a spacing of 0.35 nm – in line with the (101) spacing of the $TiO_2$ anatase phase. The small crystallite size may explain the broadening of the anatase peak in the XRD data in Figure 2a. Using the Scherrer equation for the anatase peak at $2\theta = 25.1°$ we obtain an average crystallite size of ~6.4 nm which fits well to the TEM results.

Field induced crystallization has been observed in previous work for various anodic oxides.[17,23–28] In many cases the nucleation of crystalline oxide was reported to take place in the oxide at the oxide/metal interface due to the high electric field applied to such barrier layer. This can lead to localized heating effects or nanoscopic avalanche events and consequent partial crystallization. Hence, we propose that the high field anodic process established under the present electrochemical conditions provides partially crystalline oxide and a selective dissolution process of amorphous material.[29,30]

XPS (Figure 2c–e) and EDX (Table 1) show that the titania nano-tree structure shows a significant uptake of phosphorous from the electrolyte, as also shown by the XPS survey in Figure S4. The Ti doublet (Figure 2c), with the Ti $2p_{3/2}$ and Ti $2p_{1/2}$ signals at 457.9 and 463.7 eV, respectively, fits well to $Ti^{4+}$

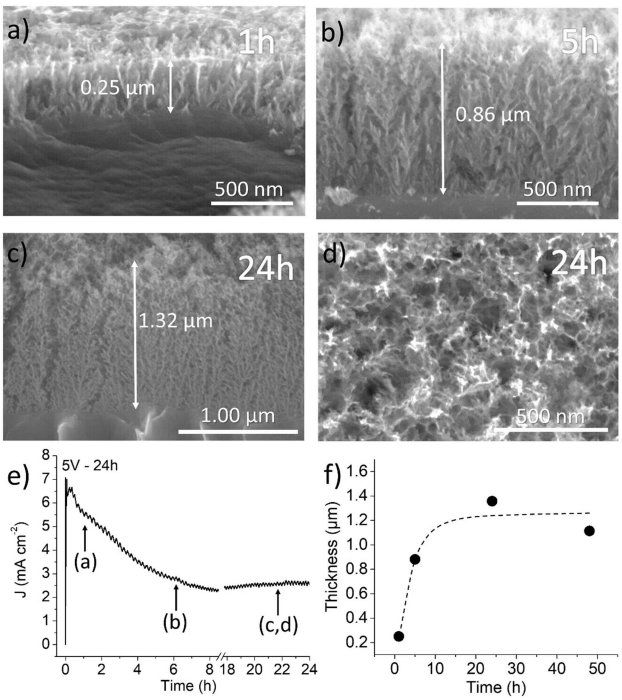


**Figure 1.** Cross sectional SEM images of anodic $TiO_2$ oxide layers formed in molten o-$H_3PO_4$ and 5 vol% EG at 5 V, 105 °C and for different anodization times: a) 1 h, b) 5 h, c) 24 h. d) Top-view SEM image and e) J-time curve of the anodic layer grown after 24 h. f) Thickness of the anodic oxide layers vs. anodization time.

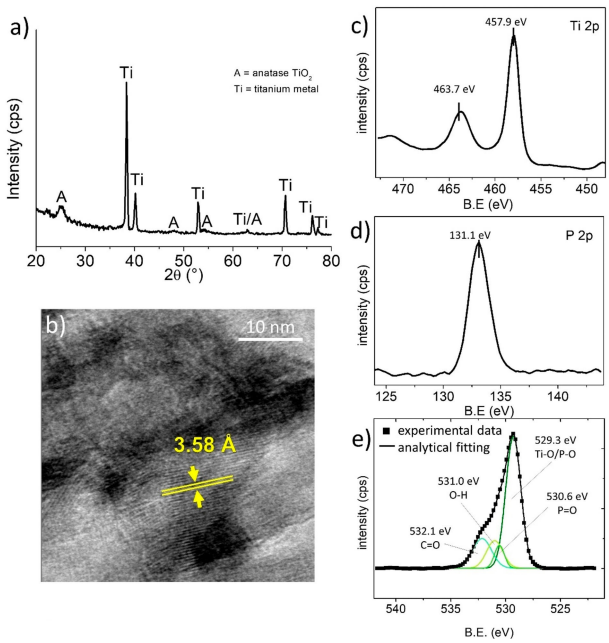


**Figure 2.** a) XRD pattern, b) HR-TEM and c–e) XPS data for an as-formed anodic layer grown in molten o-$H_3PO_4$ and 5 vol% EG at 5 V, 105 °C for 24 h. Table 1 (bottom) shows XPS and EDX composition (at %) of the as-formed anodic layer grown for 24 h.

in $TiO_2$ lattice. The location of the P2p peak at 133.1 eV (Figure 2d) is well in line with literature data on phosphates.[31] Moreover, the fitting of the oxygen peak (Figure 2e) shows the contributions of lattice Ti–O and surface O–H (hydroxyl) species, along with that of P–O and P=O species in line with the uptake of phosphate ions from the anodizing medium.[32–34]

The different nanotree layers of Figure 1 where then tested for their photocatalytic performance for the degradation of AO7. Data are compiled in Figure 3a and Figure S5). Evidently, the layer obtained after 5 h of anodization shows the highest photocatalytic degradation rate, with a first order rate constant k of $-5.1\ 10^{-3}\ h^{-1}$, corresponding to an apparent quantum efficiency AQE of (at least) ~0.00116%. It should be pointed out that here we assume that AO7 molecules undergo degradation by reaction with photo-generated holes from $TiO_2$. One valence band hole can induce the cleavage of the N=N diazo bond of the AO7 molecule. Note that, due to their non-selective nature, photo-generated holes can react further with fragments of AO7 molecules, and photo-promoted conduction band electrons can also cause AO7 degradation (or decomposition of AO7 fragments) via formation of radicals (e.g. $O_2^{-\bullet}$), hence leading in principle to higher quantum efficiency values. These latter reaction paths were however not quantified as the spectrophotometric measurements allow only to determine the number of AO7 molecules that undergo cleavage of the N=N diazo bond, causing the loss of the typical AO7 optical absorption band at ~486 nm, i.e. causing bleaching of the reaction solution (see details in Supporting Information).

As discussed above, XPS results indicate the presence on the oxide surface of phosphates or similar P species. The role of P species on the photocatalytic performance of $TiO_2$ (or other metal oxide semiconductors) is debated in the literature.[35–38] P-doping is in some reports proposed to increase the surface area of sol-gel prepared $TiO_2$ powders (with consequent activity enhancement), while other studies concluded that P-doping may induce band gap narrowing in anatase $TiO_2$, hence limiting the photocatalyst light absorbance. Thus, whether the effect of surface adsorbed or dopant P species is positive or detrimental is not fully clear in the literature.

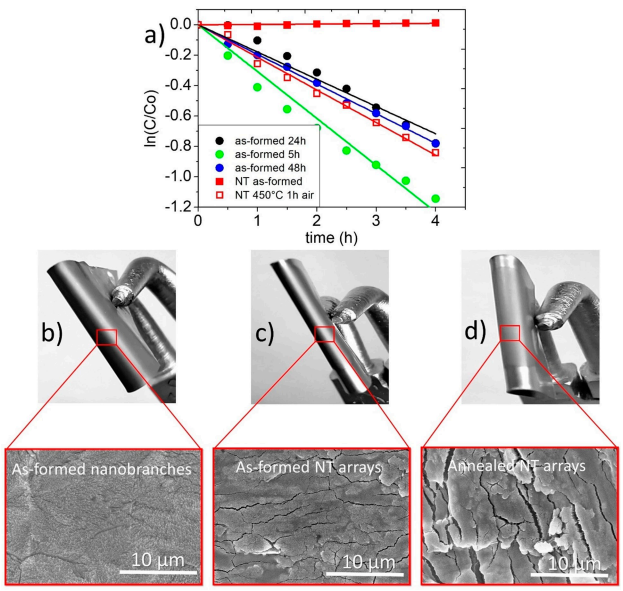


**Figure 3.** a) AO7 photo-degradation under UV light illumination for different anodic structures showing the influence of anodization time (5 h, 24 h or 48 h) for as-formed branched $TiO_2$ structure, as-formed NTs and annealed NTs. Optical and SEM images showing the effect of bending test for b) as-formed nano-branched $TiO_2$ layers, c) as-formed NTs and d) annealed NTs.

Though the hierarchical structures we compare in Figure 3 feature P on the surface likely due to adsorbed phosphates, these species are however not considered as essential for the photocatalytic performance but rather the nanocrystalline anatase structure along with the high surface area (discussed below).

To compare the obtained rates to a well-established photocatalyst geometry and structure, we compared the data with measurements carried out for comparable $TiO_2$ nanotube layers of about 2 µm thickness (as formed amorphous $TiO_2$ and fully annealed to anatase), as described in the SI (Figure S6).

Remarkably, the as-formed nanotree-structure introduced in this work outperforms not only as-formed nanotubes but even nanotube layers that were fully crystallized to anatase by a thermal treatment in air at 450 °C. Such annealing conditions are the most optimized for the photocatalytic performance of $TiO_2$ nanotubes as reported in previous work.[1,2,4] This suggests that particularly the surface area of the self-ordered nanotree structure along with the anatase crystallinity is responsible for the higher performance.

To assess the electrochemically active surface area, we carried out potentiodynamic cyclic voltammetry experiments for the different nanotree structures in an aqueous electrolyte containing a $Fe^{2+}/Fe^{3+}$ redox couple. Data are shown in Figure S7 and details are available in the Experimental Section. From the height of the peak current, we deduced the surface area and found that the latter and the photocatalytic activity correlate well (Figure S7 and Figure 3a).

As a side remark, trying to enhance the performance of the nanotree layer by additional annealing led to a worse performance than observed for the as-formed layer (Figure S8a). This can be explained by a morphology deterioration caused by the heat treatment, that leads to a sintering of the finest branches of the nanostructure (compare b) and c) in Figure S8).

This indicates that the present hierarchical structures already in their as formed state are a very potent photocatalyst that could even be applied for polymer based substrates where T < 150 °C are generally required.

The suitability of these layers for flexible substrates is evident when the bending stability of the oxide layer is assessed in a simple test as depicted in Figure 3b–d. Even when bending the substrate with plyers, the hierarchical anodic oxide layer produced here shows a very good adhesion and after bending, no fissures can be observed by SEM in the region of highest stress – note that the fissures visible in the SEM image in Figure 3b correspond in fact not to strain induced cracks but to grain boundaries. This, in contrast to as-formed nanotube layers (of comparable thickness e.g. ~1 or 2 µm thick – see Figure 3c and Figure S9a, b), not to mention the typically brittle

annealed nanotube layers, where μm-wide cracks are formed under the same test conditions (Figure 3d and Figure S9c).

Overall, the present work therefore shows that a simple anodization process of titanium in a hot phosphoric acid/ethylene glycol electrolyte can directly lead to a highly photocatalytically active layer that consists of a hierarchical structure containing embedded anatase crystallites. This layer outperforms comparable layers of $TiO_2$ nanotubes, even if they are in their most active fully crystalline anatase state. Moreover, the layers have a remarkable bending stability, which makes them highly promising for applications in flexible polymer substrate based photocatalytic devices.

## 3. Conclusions

We introduced an anodization procedure of titanium based on the use of an electrolyte composed of molten phosphoric acid and small contents of ethylene glycol. Anodization at temperatures as low as ~100 °C allows to produce high surface area, hierarchical $TiO_2$ layers that adhere excellently to the Ti substrate. We show that these anodic layers are partially crystalline already in the as-formed state, i.e. they provide embedded anatase nanocrystals throughout the anodic structure and therefore do not require any further thermal treatment for providing an excellent photocatalytic performance. Such structures were found to be more active for the photocatalytic degradation of a model pollutant (AO7) than comparable as-formed or even annealed anodic $TiO_2$ nanotube layers. The nanocrystalline nature along with the excellent mechanical robustness makes such anodic layers promising for flexible photocatalytic or photo-electrode surfaces.

## Experimental Section

### Anodic Growth

Titanium foils (15×15 $cm^2$, 0.125 mm thickness, 99.5% purity, obtained from Advent Research Material LDT, Oxford, UK) were cut into 2×1.5 $cm^2$ samples, degreased and cleaned by ultra-sonication in acetone, ethanol and de-ionized (DI) water (15 min each step) and finally dried in a $N_2$ stream.

The anodization experiments to grow the hierarchical $TiO_2$ nanostructures were carried out in a vertical two-electrode electrochemical cell configuration. A Ti sample and a Pt sheet were the working electrode (anode) and the counter electrode (cathode), respectively. The two electrodes, spaced 2 cm apart, were immersed in an anodizing medium composed of a solution of molten orthophosphoric acid (o-$H_3PO_4$, ≥99%, Sigma-Aldrich). In previous work we explored electrolytes based on o-$H_3PO_4$ with the addition of high concentrations of HF[39] or used as pure anodizing medium.[40–42] Here we incorporate to molten o-$H_3PO_4$ 5 vol% ethylene glycol (EG, Fluka Analytical, ≥99.5%). The electrolyte was placed on a heated stirring plate (IKA C-MAG A57) equipped with a thermostatic controller, and was constantly stirred with a magnetic bar and kept at a constant temperature of 105 °C. The thermocouple was fully wrapped into Teflon tape, in order to protect the steel probe from the acid solution. Prior to anodization, the electrolyte was held at the desired temperature for 30 min. The experiments were performed under potentiostatic condition, that is, by applying for 1–48 h a constant DC potential of 5 V provided by an external power supply (VOLTCRAFT VLP 2403 Pro). The resulting current density was recorded by using a Keithley 2100 multimeter interfaced with a laptop. After the anodization process the samples were immersed in ethanol for 30 min to remove the residual electrolyte. Subsequently, the samples were dried in a $N_2$ stream.

As reference materials, a set of $TiO_2$ nanotube layers were grown by anodization of titanium sheets (0.125 mm thick, Advent Research Materials, 99.6+% purity) in an ethylene glycol-based solution containing 0.15 M $NH_4F$ and 3 vol% deionized water, at 60 V in an O-ring electrochemical cell. Also, in this two-electrode setup, a platinum sheet was used as a cathode and counter electrode. All experiments where performed under ambient temperature (ca. 18–22 °C). The structures were grown for 3.5 minutes to reach a NT layer thickness of ca. 2 μm. The samples were afterwards kept in ethanol overnight and finally dried with $N_2$. These layers were then crystallized to anatase phase by a thermal treatment at 450 °C for 1 h in air using a tubular furnace.

### Characterization of Anodic $TiO_2$ Nanostructures

A Hitachi field emission scanning electron microscope (FE-SEM S4800, Hitachi) and a high resolution transmission electron microscope (HR-TEM, Philips CM300) were used for morphological characterization of the samples. The thickness of the anodic films was obtained by SEM either by scratching off the layer with a metal scalpel or by bending the sample substrates. For TEM investigations, the samples were mechanically scratched from the substrate and the resulting powder was deposited on a copper TEM grid.

The chemical features of the $TiO_2$ branched nanostructures were analyzed by X-ray photoelectron spectroscopy (XPS, PHI 5600 Multi-Technique System, US) equipped with a monochromatic Al Kα X-ray source (1486.6 eV). Further chemical analysis were performed by energy-dispersive X-ray spectroscopy (EDAX Genesis, fitted to SEM chamber). X-ray diffraction (XRD) analysis was carried out using an X'pert Philips PMD diffractometer with a Panalytical X'celerator detector, using graphite-monochromized Cu Kα radiation (λ = 1.54056 Å). The electrochemically available surface area of the different nanotree structures was assessed by potentiodynamic cyclic voltammetry in an aqueous electrolyte containing a $Fe^{2+}$/$Fe^{3+}$ redox couple. The electrolyte contained 0.5 mM $K_4Fe(CN)_6$ (Merck, Germany),0.5 mM $K_3Fe(CN)_6$ (Carl Roth GmbH, Germany) and 0.5 M KCl (Sigma). The j-V curves were measured with an Autolab setup (Metrohm, Switzerland) using Nova software, in a two electrode configuration with the nanotree layer as the working electrode and a Pt foil as counter electrode. The potential was cycled in the −0.7–+0.8 V range. The sweep rate was 100 mV $s^{-1}$. 10 j-V cycles were recorded for each samples to equilibrate the system. The data in Figure S7 are relative to the 10$^{th}$ cycle of each sample.

### Photocatalytic Experiments

For testing the photocatalytic oxidation ability of the different anodic $TiO_2$ nanostructures we used as a test reaction the decomposition of a model organic pollutant, i.e. acid orange 7 (AO7). For this, the samples were immersed in a quartz glass cuvette (reaction cuvette) with optical path of 10 mm containing 3 mL of an aqueous AO7 solution. The dye initial concentration ($C_0$) was 2.5 $10^{-5}$ M. The illumination was provided by an UV-LED emitting at 365 nm (power density 100 mW $cm^{-2}$). The illuminated sample surface was 1 $cm^2$.

Every 30 minutes, a sample of about 500 μL of AO7 solution was withdrawn with a syringe to determine the solution absorbance with a UV/VIS spectrophotometer (LAMBDA XLS, Perkin-Elmer) at $\lambda = 486$ nm. This wavelength corresponds to the peak of maximum absorbance of AO7. The solution absorbance was correlated to the AO7 residual concentration by using the Lambert-Beer law. A high precision quartz cuvette (Quartz Suprasil® Hellma Analytics) was used, with a length path of 10 mm. Each absorbance measurement took less than a minute. Immediately after the measurement, the withdrawn sample was put back in the reaction cuvette.

For the evaluation of the solar light activity, the system was irradiated with AM 1.5 simulated solar light (100 mW $cm^{-2}$) provided by a solar simulator (300 W Xe lamp power supply, with optical solar light filter).

## Acknowledgements

*M.A. and P.S. would like to acknowledge the ERC, DFG and the DFG cluster of excellence EAM for financial support. The authors would like to acknowledge the support of the Center for Nanoanalysis and Electron Microscopy (CENEM, University of Erlangen-Nuremberg) and Nikita Denisov for the morphological TEM analysis and for helping with data evaluation. Helga Hildebrand and Dr. Anca Mazare are acknowledged for technical help with the XPS analysis and data processing. Seyedsina Hejazi is acknowledged for technical help with the potentiodynamic cyclic voltammetry measurements. Open access funding enabled and organized by Projekt DEAL.*

## Conflict of Interest

The authors declare no conflict of interest.

**Keywords:** anodization · ortho-phosphoric acid · $TiO_2$ · hierarchical nanostructure · photocatalysis

[1] K. Lee, A. Mazare, P. Schmuki, *Chem. Rev.* **2014**, *114*, 9385.
[2] P. Roy, S. Berger, P. Schmuki, *Angew. Chem. Int. Ed.* **2011**, *50*, 2904.
[3] H. Tsuchiya, P. Schmuki, *Nanoscale* **2020**, *12*, 8119.
[4] I. Paramasivam, H. Jha, N. Liu, P. Schmuki, *Small* **2012**, *8*, 3073.
[5] X. Zhou, N. Liu, P. Schmuki, *ACS Catal.* **2017**, *7*, 3210.
[6] M. Altomare, N. T. Nguyen, P. Schmuki, *Chem. Sci.* **2016**, *7*, 6865.
[7] K. Zhu, T. B. Vinzant, N. R. Neale, A. J. Frank, *Nano Lett.* **2007**, *7*, 3739.
[8] J. R. Jennings, A. Ghicov, L. M. Peter, P. Schmuki, A. B. Walker, *J. Am. Chem. Soc.* **2008**, 13364.
[9] F. Mohammadpour, M. Moradi, K. Lee, G. Cha, S. So, A. Kahnt, D. M. Guldi, M. Altomare, P. Schmuki, *Chem. Commun.* **2015**, *51*, 1631.
[10] S. Bauer, P. Schmuki, K. von der Mark, J. Park, *Prog. Mater. Sci.* **2013**, *58*, 261.
[11] J. Park, S. Bauer, P. Schmuki, K. von der Mark, *Nano Lett.* **2009**, *9*, 3157.
[12] A. L. Linsebigler, G. Lu, J. T. Yates, *Chem. Rev.* **1995**, *95*, 735.
[13] S. Malato, P. Fernández-Ibáñez, M. I. Maldonado, J. Blanco, W. Gernjak, *Catal. Today* **2009**, *147*, 1.
[14] M. N. Chong, B. Jin, C. W. K. Chow, C. Saint, *Water Res.* **2010**, *44*, 2997.
[15] U. I. Gaya, A. H. Abdullah, *J. Photochem. Photobiol. C* **2008**, *9*, 1.
[16] Y.-M. Li, L. Young, *J. Electrochem. Soc.* **2001**, *148*, B337.
[17] B. Melody, *Electrochem. Solid-State Lett.* **1999**, *1*, 126.
[18] D. Kim, K. Lee, P. Roy, B. I. Birajdar, E. Spiecker, P. Schmuki, *Angew. Chem.* **2009**, *121*, 9490.
[19] D. Kuang, J. Brillet, P. Chen, M. Takata, S. Uchida, H. Miura, K. Sumioka, S. M. Zakeeruddin, M. Grätzel, *ACS Nano* **2008**, *2*, 1113.
[20] X. Zhou, N. T. Nguyen, S. Özkan, P. Schmuki, *Electrochem. Commun.* **2014**, *46*, 157.
[21] F. Riboni, N. T. Nguyen, S. So, P. Schmuki, *Nanoscale Horiz.* **2016**, *1*, 445.
[22] H. Masuda, K. Fukuda, *Science* **1995**, *268*, 1466.
[23] D. M. Lakhiani, L. L. Shreir, *Nature* **1960**, *188*, 49.
[24] H. Asoh, H. Odate, S. Ono, *J. Surf. Finish. Soc. Japan* **2004**, *55*, 952.
[25] H. Habazaki, T. Ogasawara, H. Konno, K. Shimizu, S. Nagata, P. Skeldon, G. E. Thompson, *Corros. Sci.* **2007**, *49*, 580.
[26] D. Kim, K. Lee, P. Roy, B. I. Birajdar, E. Spiecker, P. Schmuki, *Angew. Chem. Int. Ed.* **2009**, *48*, 9326.
[27] K. Lee, D. Kim, P. Roy, I. Paramasivam, B. I. Birajdar, E. Spiecker, P. Schmuki, *J. Am. Chem. Soc.* **2010**, *132*, 1478.
[28] K. Lee, D. Kim, P. Schmuki, *Chem. Commun.* **2011**, *47*, 5789.
[29] Y. Oikawa, T. Minami, H. Mayama, K. Tsujii, K. Fushimi, Y. Aoki, P. Skeldon, G. E. Thompson, H. Habazaki, *Acta Mater.* **2009**, *57*, 3941.
[30] M. Altomare, G. Cha, P. Schmuki, *Electrochim. Acta* **2020**, *344*, 136158.
[31] J. F. Moulder, W. F. Stickle, P. E. Sobol, K. D. Bomben, *Handbook of X-ray Phoelectron Spectroscopy* **1995**, J. Chastain, R. C. Jr. King, 58–59.
[32] Y. Oikawa, K. Fushimi, Y. Aoki, H. Habazaki, In *ECS Trans.*, ECS, **2008**; Vol. 16, pp. 345–351.
[33] S. Ono, N. Masuko, *ECS Trans.* **2017**, *75*, 23.
[34] G. C. Wood, P. Skeldon, E. Thompson, K. Shimizu, *J. Electrochem. Soc.* **1996**, *143*, 74.
[35] R. Marschall, L. Wang, *Catal. Today* **2014**, *225*, 111.
[36] N. Ohtsu, S. Komiya, K. Kodama, *Thin Solid Films* **2013**, *534*, 70.
[37] N. Ohtsu, D. Ishikawa, S. Komiya, K. Sakamoto, *Thin Solid Films* **2014**, *556*, 247.
[38] K. Yang, Y. Dai, B. Huang, *J. Phys. Chem. C* **2007**, *111*, 18985.
[39] J. E. Yoo, K. Lee, M. Altomare, E. Selli, P. Schmuki, *Angew. Chem. Int. Ed.* **2013**, *52*, 7514.
[40] M. Altomare, O. Pfoch, A. Tighineanu, R. Kirchgeorg, K. Lee, E. Selli, P. Schmuki, *J. Am. Chem. Soc.* **2015**, *137*, 5646.
[41] K. K. Upadhyay, M. Altomare, S. Eugénio, P. Schmuki, T. M. Silva, M. F. Montemor, *Electrochim. Acta* **2017**, *232*, 192.
[42] K. K. Upadhyay, G. Cha, H. Hildebrand, P. Schmuki, T. M. Silva, M. F. Montemor, M. Altomare, *Electrochim. Acta* **2018**, *281*, 725.

Manuscript received: May 12, 2020
Revised manuscript received: June 6, 2020
Accepted manuscript online: June 8, 2020